EXPERIMENTAL MEASUREMENTS AND CFD RESULTS OF LIQUID FILM THICKNESS IN VERTICAL DOWNWARD AIR–WATER ANNULAR FLOW

Y. RIVERA, J.L. MUÑOZ-COBO, A. ESCRIVÁ, C. BERNA & Y. CÓRDOVA
Instituto de Ingeniería Energética, Universitat Politècnica de València, Spain.

ABSTRACT

Annular gas–liquid flows have been extensively studied over the years. However, the nonlinear behavior of the interface is still currently the subject of study by multiple researchers worldwide. The appearance of a liquid layer on the wall and its turbulent behavior support the heat exchange of multiple systems in the industrial field. Research in this area allows the optimization of these installations as well as the analysis of possible safety problems if the liquid film disappears. This study first shows some of the most important findings obtained in the GEPELON experimental facility (GEneración de PElícula ONdulatoria or Wavy Film Generator). The facility was built in order to analyze the behavior of the liquid film in annular downward air–water flow. The experimental range of the inlet conditions is 800–8000 for the Re_L and 0–110,000 for the Re_g. Measurements for the mean film thickness show a fairly good agreement with the empirical correlations and the measurements of other authors. One of the most demanded applications of this type of measurements is the validation of computational dynamics or CFD codes. Therefore, the experiment has been modeled using Ansys CFX software, and the simulation results have been compared with the experimental ones. This article outlines some of the reasons why two-phase flow simulations are currently challenging and how the codes are able to overcome them. Simulation predictions are fairly close to the experimental measurements, and the mean film thickness evolution when changing the boundary conditions also shows a good agreement.

Keywords: CFD simulation, conductance probe, experimental measurements, film thickness, vertical downward annular flow.

1 INTRODUCTION

The gas–liquid annular flow appears in multiple applications in the industrial field, and its behavior has been of interest to researchers. Both natural and forced annular flow can be found in multiple installations, such as condensers, evaporators, distillation towers, or nuclear reactors. In the nuclear field, we can highlight the appearance of downward annular flow in accident scenarios for both pressurized water reactor (PWR) and boiling water reactor (BWR).

The characteristic liquid film observed near the pipe wall provides to this flow important properties, specifically those related to heat transfer. The appearance of interfacial waves in this liquid film and the high turbulence observed in the form of eddies increase the exchange of mass and heat. Multiple authors have focused their study on the behavior of these waves such as [1] and [2] and more recent articles, for instance [3, 4]. Interfacial waves can be classified into three main groups: disturbance waves (DWs), ripple waves (RWs), and ephemeral waves [5]. DWs are the largest waves with the longest lifetime, and they are characterized by occupying the entire annulus of the pipe. On the other hand, RWs are smaller, non-coherent waves that appear between the DWs and are usually absorbed by them. The ephemeral waves

© 2022 WIT Press, www.witpress.com
ISSN: 2046-0546 (paper format), ISSN: 2046-0554 (online), http://www.witpress.com/journals
DOI: 10.2495/CMEM-V10-N2-93-103

are intermediate in size between DWs and RWs, are non-coherent all around the pipe section, and generally travel between DWs until they are absorbed by them.

Many other authors have investigated the behavior of the liquid film under both upward and downward annular flow conditions where we highlight [6–9] or [10] among others. As a consequence of the exhaustive measurements carried out by different researchers, a large number of correlations have been described to obtain the value of some of the properties of the liquid film. In the case of free-fall annular flow, multiple expressions have been proposed over the years to obtain the mean film thickness. Some of these correlations can be found in [11–14]. Other authors [15–18], although they have not calculated experimental correlations, do show a large number of experimental measurements.

Although mean film thickness is the most studied variable, many other characteristics have been analyzed. Some of them have been measured, but more research effort is needed to complete the range of application as well as to propose empirical correlations. In general, most of the authors measure the average height, the frequency, and the celerity of both DWs and RWs.

CFD codes have been increasing their applications in two-phase flow over the years, although their use still represents a challenge in many of them [19]. The information available is becoming more and more extensive, but the high confidence requirements needed in some of the applications reduce their use. In the field of nuclear safety, CFD codes have a promising future [20] although a major contribution is still needed from the scientific community.

This article is structured as follows. Section 2 shows the information related to the experimental setup detailing the boundary conditions and the measurement systems. Section 3 covers the CFD model that has been generated to carry out the simulations and provides details of the methodology. Section 4 contains the discussion of the results showing the most important experimental measurements and the simulations carried out. Finally, the article ends with the main conclusions obtained that summarize the most important parts of the study.

2 EXPERIMENTAL FACILITY

2.1 Description of the facility

GEPELON experimental facility is designed to analyze the behavior of the liquid film in annular downward air–water flow (Fig. 1). The installation has two separate circuits that are joined together in the injector of the test section. On one hand, the water circuit is designed to pump water with known temperature, flow, and pressure characteristics to the injector, located in the upper part of the installation. On the other hand, the air circuit is composed of the compressor and the measurement and control systems that send a controlled airflow to the second inlet of the injector. Sensors in both circuits collect the information and send it to the data acquisition system (DAQ) where it is stored at a frequency of 2 Hz.

The water accumulated in the injector crosses through a porous pipe and joins the airflow, forming a liquid film. Both fluids flow down the test section consisting of a transparent MMA pipe equipped with multiple conductance probes. The time evolution of the liquid film obtained by these sensors is recorded in the DAQ at a frequency of 5000 Hz.

Both the injector and the test section have been duplicated, so the behavior of the film can be studied in two pipes of diameters and 42 and 30 mm. The test section is approximately 5 m long in both cases. A total of five conductance probes have been installed at 180,785,1128,2500, and 3500 mm from the inlet. For the 30-mm section, which is the one simulated with the CFD

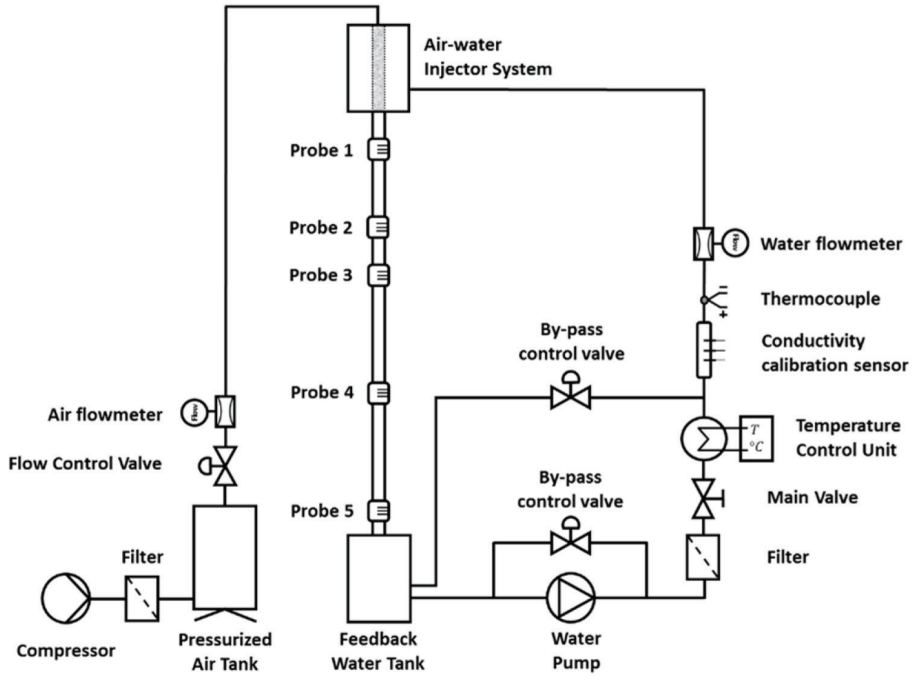

Figure 1: Flow diagram of the GEPELON facility [21].

Table 1: Inlet conditions of the liquid and gas for the experiments in the GEPELON facility.

	Flow [l/min]	**Velocity [m/s]**	**Reynolds number**
Water	1–10	0.02–0.24	800–8000
Air	0–2500	0–60	0–110,500

code, the equivalent diameters of the positions with respect to the inlet are 6, 26, 38, 83, and 117 diameters. The inlet conditions of this facility are summarized in Table 1.

2.2 Conductance probes

Conductance probes are sensors designed to measure the thickness of a thin liquid film. Their operation is based on the conductivity of water so that the current between two electrodes will be higher when the thickness of the film increases [22]. This technique has been used by a large number of authors [12, 23–29].

Among the different types of conductance probe configurations, GEPELON facility probes consist of three flush-mounted electrodes (emitter, receiver, and ground) placed at a specific spacing and diameter. The probes have been designed to have enough sensitivity without compromising the maximum saturation liquid film value (Fig. 2). The transmitting electrode sends a 100 kHz, 5 Vpp sinusoidal signal to the receiving electrode. The ground electrode is placed in the middle of both, providing stability and controlling the signal.

The electronic device that controls the electric current through the probe is composed of multiple amplifiers, a rectifier, and an electronic low-pass filter. The probe output signal is therefore rectified and amplified, so it reaches the data acquisition card as clean as possible.

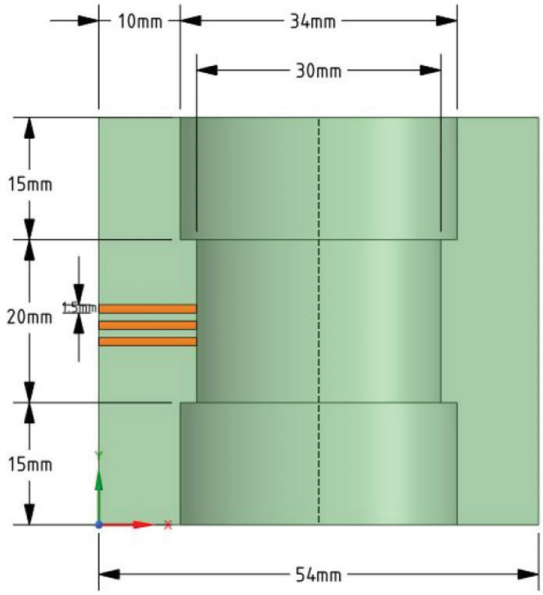

Figure 2: Conductance probes' design and dimensions.

There is a relationship between the current passing through the electrodes and the amplitude of the liquid film. In order to determine this relation, it is necessary to calibrate the probes. For this purpose, a calibration system has been developed consisting of a signal generator, the electronic circuit, a flatness table equipped with a high-accuracy positioning system, and a position coordinate display. The probe is calibrated using precise dielectric cylinders that simulate a film of known thickness. To ensure that the measurements are constant and stable, treated water is used, maintaining a conductivity value of 50 μS. The calibration system places a dielectric cylinder of known diameter in the center of the probe creating a liquid ring of known thickness. The output signal is collected by the data acquisition card, and the thickness-voltage relationship is obtained for a total of 20 calibration points. More information about the calibration system can be found in [29], where each of the devices in the system is detailed. Equation (1) is obtained adjusting the measurement points with a 5th-order polynomial.

$$h = 0.111V^5 - 0.6598\ V^4 + 1.5582\ V^3 - 1.6682V^2 + 1.2919\ V + 0.0275, \tag{1}$$

where V is the output voltage obtained and h is the thickness of the film.

3 CFD MODEL

The CFD model has been developed in ANSYS CFX® software. To simplify the case in the first stage, a reduced domain has been generated when compared to the test section of the experiment. Figure 3a shows the 300-mm geometry and 30-mm diameter that has been created for this study.

The mesh generated with the ICEM CFD® tool contains 0.6 million hexahedral elements, positioned in the flow direction. Special care has been taken in the nodes close to the wall where the interface between water and air will be located. Figure 3b and c shows the details of the upper part of the pipe and the inlet. In order to determine the mesh quality, we have followed the recommendations of CFD best practice guidelines [20] and the Ansys Meshing User Manual [30].

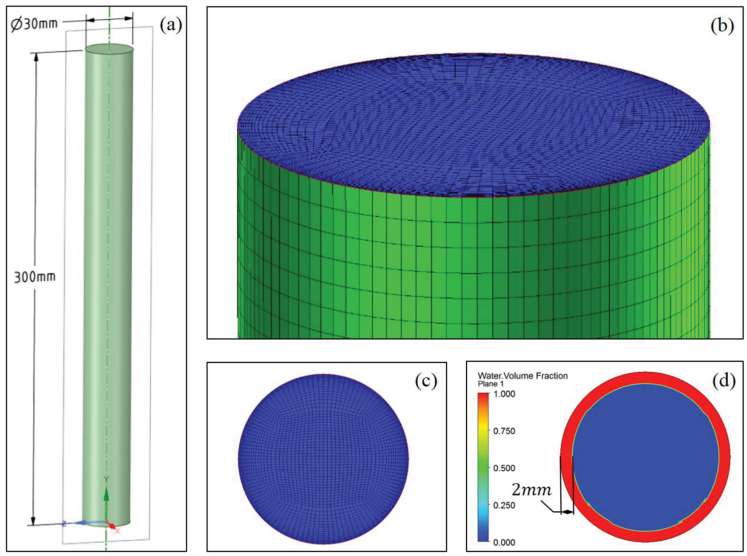

Figure 3: GEPELON model. (a) Fluid domain and dimensions, (b) detail of the top part of the cylinder mesh, (c) detail of the inlet mesh, and (d) water volume fraction at the inlet.

A total of 27 steady-state simulations have been carried out covering the range of Re_L from 800 to 6600 and Re_g from 0 to 44,000. Shear-stress transport (SST) turbulence model has been selected to decrease the computational time and to obtain values closer to the fully developed zone of the experimental facility. This model allows multiple simulations to be carried out in a short period of time at the cost of reduced accuracy for such a thin film. The large--eddy simulation (LES) model represents a more realistic option [31], but due to the high computational cost, it has been decided to reserve this option for a more advanced stage of the study. The buoyancy model selected is the density difference and the high-resolution technique as the advection scheme.

Figure 3d shows the volume fraction of the liquid in the inlet. A volume fraction profile has been generated following eqn (2).

$$VF_{water} = \begin{cases} 1 \ if \ \sqrt{x^2 + z^2} \geq r_{\text{int}} \\ 0 \ if \ \sqrt{x^2 + z^2} < r_{\text{int}} \end{cases}, \tag{2}$$

where x^2 and z^2 are the radial coordinates with the origin at the center of the pipe, and r_{int} is an arbitrary value of internal radius. This value has been set in all simulations to 0.013 m, representing a virtual liquid film thickness of 2 mm. The initial values of the variables in the domain correspond to an air volume fraction of 1 moving downward at a uniform velocity similar to the gas inlet velocity.

4 RESULTS

The liquid film in annular downward air–water flow can be analyzed from multiple perspectives. Some of the most interesting variables are the mean film thickness (h_{mean}), DW height and frequency (h_{DW}, v_{DW}), DW celerity (c_{DW}), RW height and frequency (h_{RW}, v_{RW}), or the base unperturbed film thickness (h_{bun}) among others, as shown in Fig. 4a.

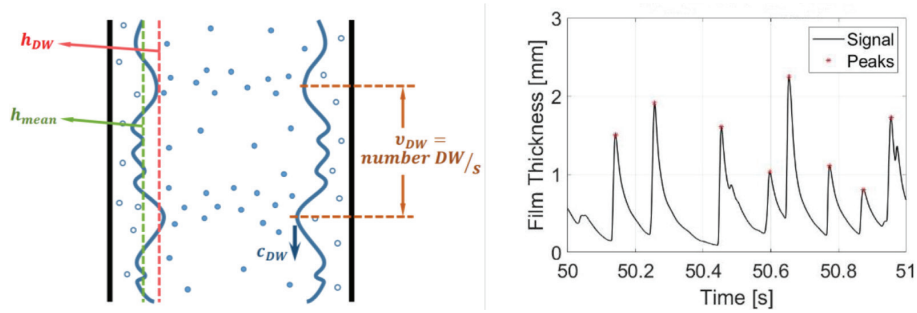

Figure 4: Main properties and evolution of the liquid film. (a) Spatial evolution of the liquid film and representation of some of the most important variables. (b) Time evolution of the film thickness and DW peaks detected.

GEPELON facility has been in operation for the last few years, and some of the results already published can be found at [21]. Data processing has recently been completed, and multiple correlations have been obtained addressing many of the liquid film variables. In this article, the analysis has been focused on the mean film thickness (h_{mean}) since it is the simplest variable to analyze from the point of view of simulations using a RANS turbulence model. Figure 4b shows the time evolution of the liquid film obtained in the experimental setup with $Re_L = 2200$ and $Re_g = 0$. The average of the signal obtained over time will be the mean film thickness.

Regarding the simulation, the liquid volume fraction has been used as a variable to obtain the average film thickness. However, there is a diffuse zone that occupies multiple cells where the volume fraction goes from 1 to 0 and where the interface is located. There are different methods to approach this problem [32] although for this analysis it has been decided to simply locate the interface at the coordinates where the volume fraction is equal to 0.5. In the future, it is expected to obtain the percentage of space in the cell occupied by the liquid and

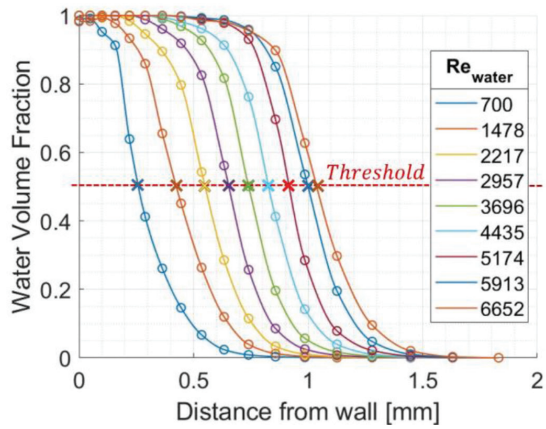

Figure 5: Water volume fraction for different Re_L depending on the distance from the wall.

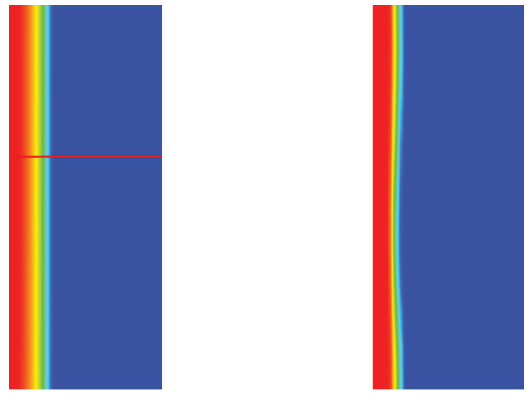

Figure 6: Liquid film in a cross-sectional plane inside the pipe. (a) RANS turbulence model simulation. (b) LES turbulence model simulation.

to collapse all the volumes into a single liquid film. Figure 5 shows the evolution of the water volume fraction with the distance to the wall for different liquid Reynolds numbers and a constant gas Reynolds number of 44,210.

The fluid film variables derived from the appearance of waves, both DWs and RWs, require the use of advanced transient simulations with more complex turbulence models such as LES or certain URANS. Simulations of this type are currently being carried out but outside the scope of this article.

A comparison of the volume fraction in a longitudinal plane inside the pipe for a time instant between the RANS and LES simulation can be seen in Fig. 6. On the left, the RANS model predicts a constant and uniform film while a long ripple is slightly observed at the interface in the LES model as well as a thinner interface. Since the pipe extension in the simulations is much smaller than that in the experiments and the DWs need a wide path to develop, it is expected not to see clear DWs at this stage. According to [33], waves are formed at the beginning of the pipe and have a high frequency. As they move down the pipe, they coalesce into larger scale DWs.

A large number of authors have studied the mean film thickness, and it is possible to find measurements for a wide range of free-falling conditions in the literature. Figure 7 shows the experimental measurements of different authors for the mean film thickness in free-fall annular flow. Continuous lines refer to the expressions of [11] and [13] widely accepted by the scientific community. The different markers correspond to experimental measurements by other authors specifying the reference, the measurement system, and the pipe diameter. First, measurements using electrical methods correspond to: [34] using conductance probes; [12] with capacitance probes; [14, 35] using parallel wire probes; and our measurements by means of flush-mounted conductance probes in the GEPELON installation [21]. On the other hand, experimental measurements using optical methods are also included such as [15] measuring kerosene with the photo-chromic dye tracer technique; and [16–18] using different variants of the laser-induced fluorescence (LIF) technique. The CFD results obtained following the model described in this article correctly predict the experimental measurements, although a more linear trend is observed than the followed by the experiments.

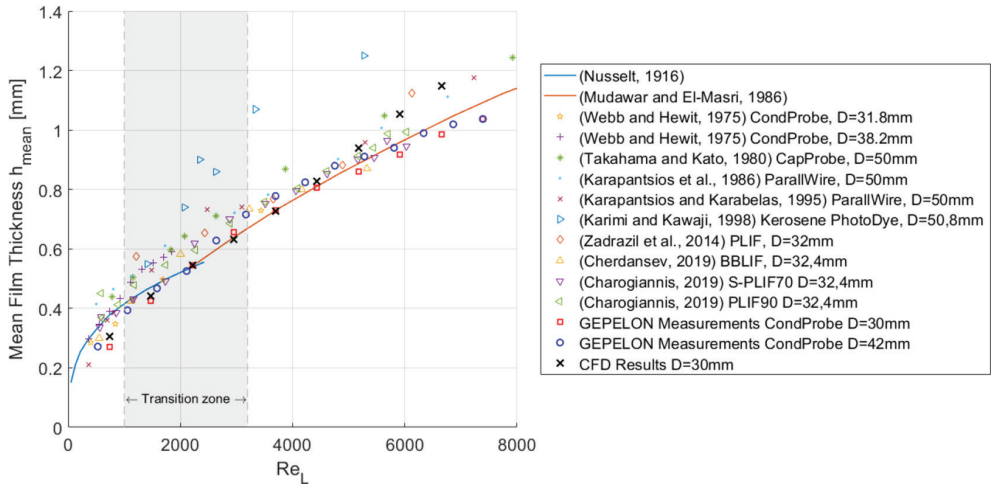

Figure 7: Comparison between experimental measurements from different authors, correlations, and CFD results. Red squares and blue cycles represent the experimental measurements, while the black crosses correspond to the CFD predictions.

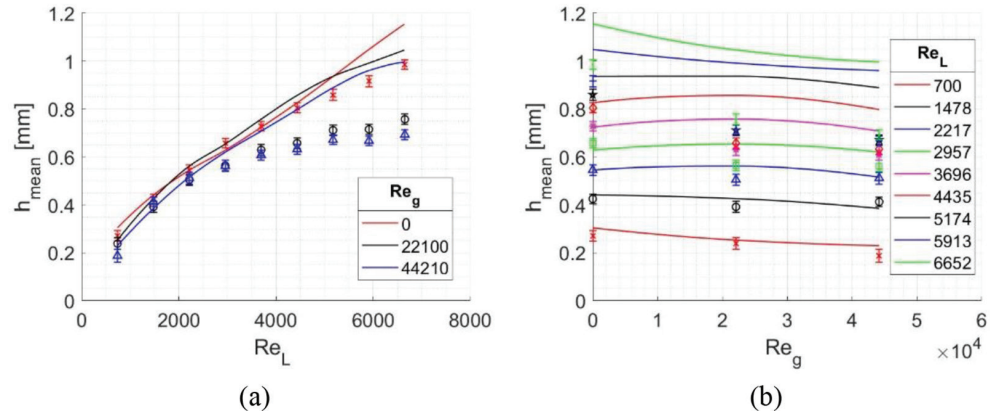

Figure 8: Comparison between experimental measurements and CFD results for downward co-current annular flow. (a) Mean film thickness vs Re_L. (b) Mean film thickness vs Re_g.

Finally, Fig. 8 shows the experimental measurements and simulation results of the average film thickness for different Re_L and Re_g. Currently, CFD results are limited to the range of Re_g between 0 and 44,210 although it is expected to increase these values to cover the full range of the experiment. As shown in the figure, there is a good agreement between simulation predictions and experiments for small Reynolds numbers of the gas, but the CFD calculations overpredict the mean film thickness for higher values.

5 CONCLUSIONS

This document summarizes the operation of the GEPELON installation, whose objective is the development of a downward annular air–water flow. The installation is equipped with

five conductance probes located at different heights and capable of measuring the time evolution of the liquid layer. By processing this signal, it is possible to obtain measurements of the mean film thickness, the height and frequency of the DWs, or the base unperturbed film height among other variables. The measurement range of this facility is 800–8000 for the liquid Reynolds number and 0–1,100,000 for the gas Reynolds number.

The CFD model of the GEPELON facility is simulated using Ansys CFX® code. In this first stage, the model has a 0.6 million nodes mesh, and it is designed to work with the SST turbulence model in steady-state simulations. A total of 27 simulations have been carried out covering the range 800–6600 for the liquid Reynolds number and 0–44,000 for gas.

The comparison of the simulation predictions with experimental measurements from different researchers and the GEPELON facility shows a fairly good agreement. For free-fall annular flow ($Re_g = 0$), a high accuracy is obtained in the CFD results although a more linear trend is observed compared to the tendency of the experiments. In relation to the co-current results with forced airflow, good agreement is observed for small Reynolds number of the liquid but the discrepancy increases for higher Re_L.

In the next stage of the investigation, it is expected to complete the CFD model to cover the full range of initial conditions of the experiment. In addition, it is planned to increase the accuracy using more complex models, such as LES turbulence model. Additionally, an uncertainty quantification analysis is expected to be carried out to include the error bands in the predictions of the CFD simulations.

ACKNOWLEDGMENT

The authors are indebted to the plan of I+D support of the EXMOTRANSIN project ENE2016-79489-C2-1-P.

REFERENCES

[1] Hanratty, T.J. & Hershman, A., Initiation of roll waves. *AIChE Journal*, **7**, pp. 488–497, 1961. https://doi.org/10.1002/aic.690070330

[2] Hall Taylor, N.S., Hewitt, I.J., Ockendon, J.R. & Witelski, T.P., A new model for disturbance waves. *International Journal of Multiphase Flow*, **66,** pp. 38–45, 2014. https://doi.org/10.1016/J.IJMULTIPHASEFLOW.2014.06.004

[3] Alekseenko, S.V., Antipin, V.A., Cherdantsev, A.V., Kharlamov, S.M. & Markovich, D.M., Investigation of waves interaction in annular gas-liquid flow using high-speed fluorescent visualization technique. *Microgravity Science and Technology*, **20**, pp. 271–275, 2008. https://doi.org/10.1007/s12217-008-9028-1

[4] Alekseenko, S.V., Cherdantsev, A.V., Cherdantsev, M.V., Isaenkov, S.V. & Markovich, D.M., Study of formation and development of disturbance waves in annular gas-liquid flow. *International Journal of Multiphase Flow*, **77**, pp. 65–75, 2015. https://doi.org/10.1016/j.ijmultiphaseflow.2015.08.007

[5] Wolf, A., *Film Structure of Vertical Annular Flow, Imperial College of Science, Technology and Medicine*. London University, 1995.

[6] Schubring, D., Ashwood, A.C., Shedd, T.A. & Hurlburt, E.T., Planar laser-induced fluorescence (PLIF) measurements of liquid film thickness in annular flow. Part I: Methods and data. *International Journal of Multiphase Flow*, **36,** pp. 815–824, 2010. https://doi.org/10.1016/j.ijmultiphaseflow.2010.05.007

[7] Belt, R.J., Van't Westende, J.M.C., Prasser, H.M. & Portela, L.M., Time and spatially resolved measurements of interfacial waves in vertical annular flow. *International Jour-*

nal of Multiphase Flow, **36,** pp. 570–587, 2010. https://doi.org/10.1016/j.ijmultiphaseflow.2010.03.004

[8] Berna, C., Escrivá, A., Muñoz-Cobo, J.L. & Herranz, L.E., Review of droplet entrainment in annular flow: Interfacial waves and onset of entrainment. *Progress in Nuclear Energy*, **74**, pp. 14–43, 2014. https://doi.org/10.1016/j.pnucene.2014.01.018

[9] Berna, C., Escrivá, A., Muñoz-Cobo, J.L. & Herranz, L.E., Review of droplet entrainment in annular flow: Characterization of the entrained droplets. *Progress in Nuclear Energy*, **79**, pp. 64–86 2015. https://doi.org/10.1016/j.pnucene.2014.11.011

[10] Setyawan, A., Indarto, Deendarlianto, The effect of the fluid properties on the wave velocity and wave frequency of gas-liquid annular two-phase flow in a horizontal pipe. *Experimental Thermal and Fluid Science*, **71**, pp. 25–41, 2016. https://doi.org/10.1016/j.expthermflusci.2015.10.008

[11] Nusselt, W., Die oberflächenkondensation des wasserdampfes. *Zeitschrift Des Vereines Dtsch. Ingenieure*, **60,** pp. 541–546 (nº27) and pp. 569–575 (nº 28), 1916.

[12] Takahama, H. & Kato, S., Longitudinal flow characteristics of vertically falling liquid films without concurrent gas flow. *International Journal of Multiphase Flow*, **6**, pp. 203–215, 1980. https://doi.org/10.1016/0301-9322(80)90011-7

[13] Mudawwar, I.A. & El-Masri, M.A., Momentum and heat transfer across freely-falling turbulent liquid films. *International Journal of Multiphase Flow*, **12**, pp. 771–790, 1986. https://doi.org/10.1016/0301-9322(86)90051-0

[14] Karapantsions, T.D., Paras, S.V. & Karabelas, A.J., Statistical characteristics of free falling films at high Reynolds numbers. *International Journal of Multiphase Flow*, **15**, pp. 1–21, 1989. https://doi.org/10.1016/0301-9322(89)90082-7

[15] Karimi, G. & Kawaji, M., An experimental study of freely falling films in a vertical tube. *Chemical Engineering Science*, **53**, pp. 3501–3512, 1998. https://doi.org/10.1016/S0009-2509(98)00159-6

[16] Zadrazil, I., Matar, O.K. & Markides, C.N., An experimental characterization of downwards gas-liquid annular flow by laser-induced fluorescence: Flow regimes and film statistics. *International Journal of Multiphase Flow*, **60**, pp. 87–102, 2014. https://doi.org/10.1016/j.ijmultiphaseflow.2013.11.008

[17] Cherdantsev, A.V., An, J.S., Charogiannis, A. & Markides, C.N., Simultaneous application of two laser-induced fluorescence approaches for film thickness measurements in annular gas-liquid flows. *International Journal of Multiphase Flow*, **119**, pp. 237–258, 2019. https://doi.org/10.1016/j.ijmultiphaseflow.2019.07.013

[18] Charogiannis, A., Sik An, J., Voulgaropoulos, V. & Markides, C.N., Structured planar laser-induced fluorescence (S-PLIF) for the accurate identification of interfaces in multiphase flows. *International Journal of Multiphase Flow*, **118**, pp. 193–204, 2019. https://doi.org/10.1016/j.ijmultiphaseflow.2019.06.002

[19] Smith, B.L., Assessment of CFD for NRS, OECD/NEA IAEA Work, 2008.

[20] Mahaffy, J., Chung, B., Dubois F., Ducros, F., Graffard, E., Heitsch, M., Henriksson, M., Komen, E., Moretti, F., Morii, T., Mühlbauer, P., Rohde, U., Scheuerer, M., Smith, B.L., Song, C., Watanabe, T. & Zigh, G., *Best Practice Guidelines for the Use of CFD in Nuclear Reactor Safety Applications*, 2014.

[21] Rivera, Y., Muñoz-Cobo, J.L., Berna, C., Escrivá, A. & Cordova, Y., Study of liquid film behaviour in vertical downward air–water annular flow. *Advances in Fluid Mechanics XIII*, pp. 77–88, 2020. https://doi.org/10.1115/1.3138339

[22] Clark, W.W.P., The interfacial characteristics of falling film reactors, pp. 1–328, 2001. http://eprints.nottingham.ac.uk/14303/ (accessed September 5, 2018)

[23] Collier, J.G. & Hewitt, G., Data on the vertical flow of air-water mixtures in the annular and dispersed flow regions, Part II: Film thickness and entrainment data and analysis of pressure drop measurements. *Trans. Inst. Chem. Eng*. **37**, pp. 127–136, 1961.

[24] Telles, A.S. & Dukler, A.E., Statistical characteristics of thin, vertical, wavy, liquid films. *Industrial & Engineering Chemistry Fundamentals*, **9**, pp. 412–421, 1970. https://doi.org/10.1021/i160035a018

[25] Fukano, T., Measurement of time varying thickness of liquid film flowing with high speed gas flow by a constant electric current method (CECM). *Nuclear Engineering and Design*, **184,** pp. 363–377, 1998. https://doi.org/10.1016/S0029-5493(98)00209-X

[26] Zhao, Y., Markides, C.N., Matar, O.K. & Hewitt, G.F., Disturbance wave development in two-phase gas–liquid upwards vertical annular flow. *International Journal of Multiphase Flow*, **55**, pp. 111–129, 2013. https://doi.org/10.1016/J.IJMULTIPHASEFLOW.2013.04.001

[27] Ghosh, S., Pratihar, D.K., Maiti, B. & Das, P.K., Automatic classification of vertical counter-current two-phase flow by capturing hydrodynamic characteristics through objective descriptions. *International Journal of Multiphase Flow*, **52**, pp. 102–120, 2013. https://doi.org/10.1016/j.ijmultiphaseflow.2012.12.007

[28] Muñoz-Cobo, J., Chiva, S., Méndez, S., Monrós, G., Escrivá, A., Cuadros, J., Muñoz-Cobo, J.L., Chiva, S., Méndez, S., Monrós, G., Escrivá, A. & Cuadros, J.L., Development of conductivity sensors for multi-phase flow local measurements at the polytechnic University of Valencia (UPV) and University Jaume I of Castellon (UJI). *Sensors*, **17**, p. 1077, 2017. https://doi.org/10.3390/s17051077

[29] Rivera, Y., Muñoz-Cobo, J.L., Cuadros, J.L., Berna, C. & Escrivá, A., Experimental study of the effects produced by the changes of the liquid and gas superficial velocities and the surface tension on the interfacial waves and the film thickness in annular concurrent upward vertical flows. *Experimental Thermal and Fluid Science*, **120**, 2021. https://doi.org/10.1016/j.expthermflusci.2020.110224

[30] Canonsburg, T.D., ANSYS meshing user' s guide. *Knowl. Creat. Diffus. Util*, **15317,** pp. 724–746, 2011.

[31] Simoneau, J.-P., Champigny, J. & Gelineau, O., Applications of large eddy simulations in nuclear field. *Nuclear Engineering and Design*, **240**, pp. 429–439, 2010. https://doi.org/10.1016/j.nucengdes.2008.08.018

[32] Iglesias, S.M., Dominguez, D.S., Escrivá, A., Muñoz-Cobo, J.L., Berna, C., Cuadros, J.L. & Rivera, Y., Computational fluid dynamics applied to the study of falling liquid films in a wave film generation facility. *Proc. 6th Eur. Conf. Comput. Mech. Solids, Struct. Coupled Probl. ECCM 2018 7th Eur. Conf. Comput. Fluid Dyn. ECFD 2018*, 2020.

[33] Fan, W., Cherdantsev, A.V. & Anglart, H., Experimental and numerical study of formation and development of disturbance waves in annular gas-liquid flow. *Energy*, **207**, p. 118309, 2020. https://doi.org/10.1016/j.energy.2020.118309

[34] Webb, D.R. & Hewitt, G.F., Downwards co-current annular flow. *International Journal of Multiphase Flow*, **2**, pp. 35–49, 1975. https://doi.org/10.1016/0301-9322(75)90027-0

[35] Karapantsios, T.D. & Karabelas, A.J., Longitudinal characteristics of wavy falling films. *International Journal of Multiphase Flow*, **21**, pp. 119–127, 1995. https://doi.org/10.1016/0301-9322(94)00048-o